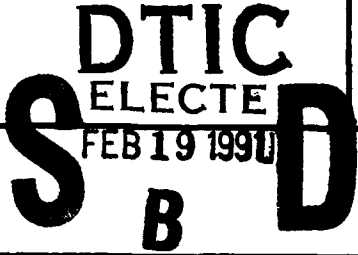


AD-A231 898

REPORT DOCUMENTATION PAGE			Form Approved OMB No. 0704-0188 (2)	
<small>Public reporting burden for this collection of information is estimated to average 1 hour per response, including the time for reviewing instructions, searching existing data sources, gathering and maintaining the data needed, and completing and reviewing the collection of information. Send comments regarding this burden estimate or any other aspect of this collection of information, including suggestions for reducing this burden, to Washington Headquarters Services, Directorate for Information Operations and Reports, 1215 Jefferson Davis Highway, Suite 1204, Arlington, VA 22202-4302 and to the Office of Management and Budget, Paperwork Reduction Project (0704-0188), Washington, DC 20503</small>				
1. AGENCY USE ONLY (Leave blank)		2. REPORT DATE		3. REPORT TYPE AND DATES COVERED Final Report/1 Nov 86-30 Apr 90
4. TITLE AND SUBTITLE Inelastic Collisional Processes of Molecules			5. FUNDING NUMBERS 61102E/2301/A4	
6. AUTHOR(S) Chun C. Lin				
7. PERFORMING ORGANIZATION NAME(S) AND ADDRESS(ES) University of Wisconsin Department of Physics Madison, WI 53706			8. PERFORMING ORGANIZATION REPORT NUMBER AFOSR-TR-91-0031	
9. SPONSORING/MONITORING AGENCY NAME(S) AND ADDRESS(ES) AFOSR/NP 36d410 Bolling AFB DC 20332-6448			10. SPONSORING/MONITORING AGENCY REPORT NUMBER AFOSR-89-0006	
				
11. SUPPLEMENTARY NOTES				
12a. DISTRIBUTION/AVAILABILITY STATEMENT Approved for public release; distribution is unlimited.			12b. DISTRIBUTION CODE	
13. ABSTRACT (Maximum 200 words) Absolute apparent cross sections for electron-impact excitation out of the 2-triplet-S metastable level of He to the 3-triplet-S, 4-triplet-S, 3-triplet-P, 3-triplet-D, 5-triplet-D, and 6-triplet D levels have been measured by a novel method. A beam of metastable atoms from a hollow-cathode discharge was crossed by an electron beam of energy from 3 to 16 eV, and the emission from the excited states was detected. Absolute calibration was made by measuring the ratio of electron excitation cross section to the known optical absorption cross section and using knowledge of the pertinent branching ratios. Direct electron-impact excitation cross sections for the 3-triplet-P, 3-triplet-S, and 3-triplet-D levels were obtained.				
14. SUBJECT TERMS electron-impact excitation, metastable atoms			15. NUMBER OF PAGES 18	
			16. PRICE CODE UL	
17. SECURITY CLASSIFICATION OF REPORT UNCLASSIFIED	18. SECURITY CLASSIFICATION OF THIS PAGE UNCLASSIFIED	19. SECURITY CLASSIFICATION OF ABSTRACT UNCLASSIFIED	20. LIMITATION OF ABSTRACT SAR	

GENERAL INSTRUCTIONS FOR COMPLETING SF 298

The Report Documentation Page (RDP) is used in announcing and cataloging reports. It is important that this information be consistent with the rest of the report, particularly the cover and title page. Instructions for filling in each block of the form follow. It is important to *stay within the lines* to meet optical scanning requirements.

Block 1. Agency Use Only (Leave blank).

Block 2. Report Date. Full publication date including day, month, and year, if available (e.g. 1 Jan 88). Must cite at least the year.

Block 3. Type of Report and Dates Covered. State whether report is interim, final, etc. If applicable, enter inclusive report dates (e.g. 10 Jun 87 - 30 Jun 88).

Block 4. Title and Subtitle. A title is taken from the part of the report that provides the most meaningful and complete information. When a report is prepared in more than one volume, repeat the primary title, add volume number, and include subtitle for the specific volume. On classified documents enter the title classification in parentheses.

Block 5. Funding Numbers. To include contract and grant numbers; may include program element number(s), project number(s), task number(s), and work unit number(s). Use the following labels:

C - Contract	PR - Project
G - Grant	TA - Task
PE - Program Element	WU - Work Unit Accession No.

Block 6. Author(s). Name(s) of person(s) responsible for writing the report, performing the research, or credited with the content of the report. If editor or compiler, this should follow the name(s).

Block 7. Performing Organization Name(s) and Address(es). Self-explanatory.

Block 8. Performing Organization Report Number. Enter the unique alphanumeric report number(s) assigned by the organization performing the report.

Block 9. Sponsoring/Monitoring Agency Name(s) and Address(es). Self-explanatory.

Block 10. Sponsoring/Monitoring Agency Report Number. (If known)

Block 11. Supplementary Notes. Enter information not included elsewhere such as: Prepared in cooperation with...; Trans. of...; To be published in.... When a report is revised, include a statement whether the new report supersedes or supplements the older report.

Block 12a. Distribution/Availability Statement. Denotes public availability or limitations. Cite any availability to the public. Enter additional limitations or special markings in all capitals (e.g. NOFORN, REL, ITAR).

DOD - See DoDD 5230.24, "Distribution Statements on Technical Documents."

DOE - See authorities.

NASA - See Handbook NHB 2200.2.

NTIS - Leave blank.

Block 12b. Distribution Code.

DOD - Leave blank.

DOE - Enter DOE distribution categories from the Standard Distribution for Unclassified Scientific and Technical Reports.

NASA - Leave blank.

NTIS - Leave blank.

Block 13. Abstract. Include a brief (*Maximum 200 words*) factual summary of the most significant information contained in the report.

Block 14. Subject Terms. Keywords or phrases identifying major subjects in the report.

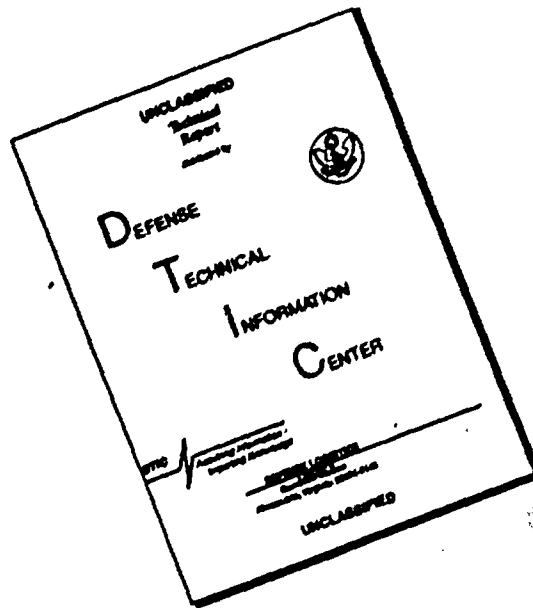
Block 15. Number of Pages. Enter the total number of pages.

Block 16. Price Code. Enter appropriate price code (*NTIS only*).

Blocks 17. - 19. Security Classifications. Self-explanatory. Enter U.S. Security Classification in accordance with U.S. Security Regulations (i.e., UNCLASSIFIED). If form contains classified information, stamp classification on the top and bottom of the page.

Block 20. Limitation of Abstract. This block must be completed to assign a limitation to the abstract. Enter either UL (unlimited) or SAR (same as report). An entry in this block is necessary if the abstract is to be limited. If blank, the abstract is assumed to be unlimited.

DISCLAIMER NOTICE



THIS DOCUMENT IS BEST QUALITY AVAILABLE. THE COPY FURNISHED TO DTIC CONTAINED A SIGNIFICANT NUMBER OF PAGES WHICH DO NOT REPRODUCE LEGIBLY.

FINAL REPORT

INELASTIC COLLISIONAL PROCESSES OF MOLECULES

AFOSR-89-0006

Chun C. Lin

University of Wisconsin

Department of Physics

Madison, WI 53706

1 November 1988 - 30 April 1990

Technical Report

Grant: AFOSR-89-0006

Period: November 1, 1988 to April 30, 1990

Principal Investigator: Professor Chun C. Lin,

Department of Physics, University of Wisconsin, Madison, WI 53706

Under the sponsorship of the Air Force Office of Scientific Research, we have conducted a study of inelastic collisional processes of molecules. The highlights of the accomplishments are as follows:

1. We have measured the cross sections for electron impact excitation out of the 2^3S metastable level of the helium atom to the 3^3S , 3^3P , 3^3D , 4^3S , and 4^3D levels. The cross sections are much larger than those for excitation out of the ground level. Based on the cross section data for excitation out of the ground level, we expect excitation out of 2^3S to 3^3P to have larger cross sections than to 3^3S and to 3^3D since $2^3S \rightarrow 2^3P$ corresponds to an optical transition. However, our measurements show the opposite, i.e., excitation from 2^3S to 3^3P is less favorable than to 3^3S and 3^3D . This indicates a fundamental difference between excitation out of the ground level and excitation out of the metastable level. Further research work should be most important for a fundamental understanding of electron excitation. Moreover the metastable atoms play an important role in many energy transfer processes. Cross sections for excitation out of the metastable levels are essential to understand many natural and laboratory phenomena. This work has been published in Physical Review Letters, Volume 62, pp. 2253-2256 (1989). Two copies of reprints are enclosed herewith.

2. We have studied electron impact excitation of the Rydberg electronic states, $x^1\Sigma_g^-$, $y^1\Pi_g$, and $o_3^1\Pi_u$ electronic states of the N_2 molecule. Measurements were made of the electron-impact optical-emission cross sections of many vibrational bands of the $y^1\Pi_g \rightarrow w^1\Delta_u$, $y^1\Pi_g \rightarrow a'^1\Sigma_u^-$, $x^1\Sigma_g^- \rightarrow a'^1\Sigma_u^-$, and $o_3^1\Pi_u \rightarrow a^1\Pi_g$ electronic transitions. The dependence of the emission cross sections of selected bands on

electron energy has been studied. The excitation functions of the $y \rightarrow a'$ and $x \rightarrow a'$ bands have similar shapes below about 50 eV with a peak near 32 eV, and are approximately proportional to $1/E$ at high energies. The $o_3 \rightarrow a$ excitation function shows a broader excitation function compared to the $y \rightarrow a'$ and $x \rightarrow a'$ excitation functions. These cross sections are very important for studying atmospheric radiation. This work has been published in Physical Review A, Volume 41, pp. 1324-1334 (1990). Two copies of reprints are enclosed herewith.



Accession For	
NTIS GRA&I	<input checked="" type="checkbox"/>
DTIC TAB	<input type="checkbox"/>
Unannounced	<input type="checkbox"/>
Justification _____	
By _____	
Distribution/	
Availability Codes	
Dist	Avail and/or Special
A-1	

Cross Sections for Electron-Impact Excitation out of Metastable Helium Levels

David L. A. Rall,^(a) Francis A. Sharpton, M. Bruce Schulman,^(b) L. W. Anderson,
J. E. Lawler, and Chun C. Lin

Department of Physics, University of Wisconsin, Madison, Wisconsin 53706

(Received 27 January 1989)

Absolute apparent cross sections for electron-impact excitation out of the 2^3S metastable level of He to the 3^3S , 4^3S , 3^3P , 3^3D , 4^3D , 5^3D , and 6^3D levels have been measured by a novel method. A beam of metastable atoms from a hollow-cathode discharge is crossed by an electron beam of energy from 3 to 16 eV, and the emission from the excited states is detected. Absolute calibration is made by measuring the ratio of electron excitation cross section to the known optical absorption cross section and using knowledge of the pertinent branching ratios. Direct electron-impact excitation cross sections for the 3^3P , 3^3S , and 3^3D levels are obtained.

PACS numbers: 34.80.Dp

This paper reports a new method for making measurements of the absolute apparent cross sections for electron excitation of He atoms out of the 2^3S metastable level to the 3^3S , 4^3S , 3^3P , 3^3D , 4^3D , 5^3D , and 6^3D levels at low He density. Also reported are the absolute cross sections for direct excitation from the 2^3S level to the 3^3P , 3^3S , and 3^3D levels. Cross sections for the electron excitation out of an excited level are of intrinsic interest in understanding excitation processes. In addition to the intrinsic interest in these cross sections, they play an important role in understanding gas discharges and related phenomena. However, few measurements of such cross sections are available,¹ although there are extensive theoretical calculations of these cross sections.²⁻⁶

In this experiment the cross sections for electron-impact excitation from the 2^3S level to the n^3L levels are determined by measuring the intensity of the radiation emitted from the n^3L levels.⁷ Figure 1 shows a schematic diagram of our apparatus. Helium atoms in the 2^3S metastable level are formed in a water-cooled intense

hollow-cathode discharge. The 2^3S metastable He atoms together with the ground-level He atoms flow out of the hollow cathode through a 1-mm-diam aperture into a large vacuum chamber that is pumped by a 6-in.-diam diffusion pump. The metastable atoms in the emerging beam have a density of about $5 \times 10^9 \text{ cm}^{-3}$ corresponding to 0.003% of the He atoms flowing out of the hollow cathode. The He beam is perpendicularly crossed by an electron beam. The electron-beam current is measured by a Faraday cup. The Faraday cup has holes cut into it to permit the He atoms to pass through the cup, to view the radiation emitted by the electron-beam-excited atoms, and to permit a laser beam to pass through the excitation region for the purpose of absolute calibration as described in this paper. A typical electron-beam current is $10 \mu\text{A}$ at 10 eV energy. The excitation region is viewed at right angles to the He-beam axis at an angle of 60° to the electron-beam axis. The light is collected by an aspheric $f/0.93$ lens, passes through an interference filter, and is focused onto the photocathode of a photomultiplier. The interference filter is used to select a transition from a particular n^3L excited level. The optical emission from the transition being studied is recorded by photon counting at various electron energies. Because the He beam is made up mostly of He atoms in the ground level, the photon counting rate due to the ground-level excitation is much larger than that due to excitation out of the metastable level for electron energies large enough that excitation from the ground level is possible. Thus the cross section out of the metastable level can be measured only at energies less than the electron energy at which excitation from the ground level of He is possible (22.7 eV). All the voltages in the electron gun are kept well below 22.7 V in order to eliminate any production of light in the electron gun which could be scattered into the photomultiplier. There is a background that results primarily from light produced in the hollow cathode and scattered by the He beam and by surfaces in the collision chamber. The signal is detected in the presence of this background by the use of off-on

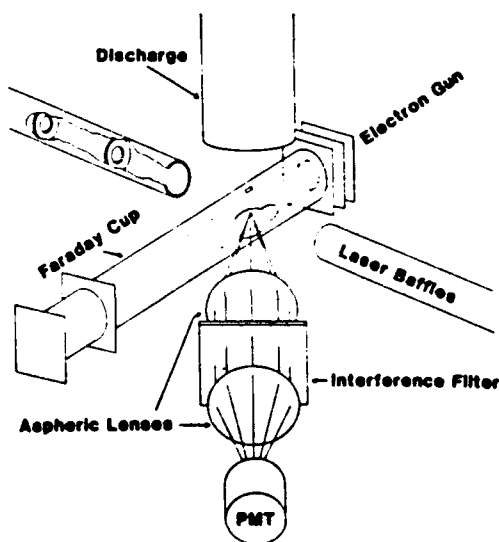


FIG. 1. Schematic diagram of the apparatus.

modulation of the electron beam. Photon counting with the electron beam on minus the counts with the electron beam off is recorded. In order to study systematic problems, the experiment is repeated except that the electron beam is off for both counting cycles. Under this condition the count-rate difference is zero within statistical accuracy. The experiment is also repeated with the discharge turned off so that there are no metastable atoms in the He beam. The count-rate difference is zero within the statistical accuracy at electron energies below 16 eV. A polarizing filter is used to check the polarization of the emitted radiation. The measured polarization is less than 5% on all lines. Because of the small value of the observed polarization, no polarization correction was made to the cross sections.

The optical signal for a particular transition produced by electron excitation from the 2^3S level per unit electron-beam length is equal to the optical emission cross section for that transition times the 2^3S metastable atom density, times the electron-beam current divided by the electron charge, and times the efficiency of the optical collection system. Thus relative optical emission cross sections for the $3^3S \rightarrow 2^3P$ (7065 Å), $4^3S \rightarrow 2^3P$ (4713 Å), $3^3P \rightarrow 2^3S$ (3889 Å), $3^3D \rightarrow 2^3P$ (5876 Å), $4^3D \rightarrow 2^3P$ (4472 Å), $5^3D \rightarrow 2^3P$ (4026 Å), and $6^3D \rightarrow 2^3P$ (3820 Å) transitions are obtained from the measured optical signals and the relative optical efficiency of our system at these seven wavelengths. The relative optical efficiencies are determined by measuring the emission signals of the same seven transitions produced by *electron excitation of the ground-level He atoms* at electron-beam energies corresponding to the peak of the excitation functions (~ 30 eV) and comparing these signals with the known optical emission cross sections for these transitions produced by *electron excitation of the ground-level He atoms*.⁸

Absolute calibration of the relative optical cross sections for the seven transitions produced by excitation out of the metastable level requires a knowledge of the product of the 2^3S metastable atom density times the absolute optical efficiency. This information is found by using the technique of laser-induced fluorescence (LIF). A very low-power, nonsaturating laser beam crosses the He-beam axis at right angles and at an angle of 60° to both the electron-beam axis and the viewing axis (see Fig. 1). The LIF from the metastable is measured as the laser wavelength is scanned across the $2^3S \rightarrow 3^3P$ absorption at 3889 Å. The LIF signal, integrated over the frequency range of the linewidth, per unit length of the laser beam is equal to $\pi r_e c$ times the known $2^3S \rightarrow 3^3P$ absorption oscillator strength, f , times the 2^3S metastable number density in the beam, times the measured laser power divided by $h\nu$, times the branching ratio for the $3^3P \rightarrow 2^3S$ emission, and times the optical efficiency, where r_e is the classical radius of the electron and c is the speed of light.⁹ Upon taking the ratio of the LIF integrated signal per unit length of the laser beam to the

optical signal of the $3^3P \rightarrow 2^3S$ transition produced by a unit length of the electron beam (as discussed in the preceding paragraph), the metastable number density and the optical efficiency cancel out. Thus the absolute optical emission cross section for $3^3P \rightarrow 2^3S$ is equal to $\pi r_e c f$ times the ratio of the electron-beam excitation signal to the LIF integrated signal, times the laser power divided by $h\nu$, times the electron charge divided by the electron-beam current, times the branching ratio for the $3^3P \rightarrow 2^3S$ transition.

We have performed a similar LIF experiment at 3965 Å ($2^1S \rightarrow 4^1P$). The results show that the density of He atoms in the 2^1S level is less than 6% of the density of He atoms in the 2^3S level.

The electron-current measurement is accomplished as follows. The electron current at an energy of 12 eV or higher is reliably determined using the Faraday cup, since the fraction of the electrons leaving the beam before the viewing region is small. At energies below 10 eV the electron beam is not always sufficiently focused so that the current measured by the Faraday cup may not be identical to the current passing through the viewing region. In order to determine the electron-beam current through the viewing region at lower energies, we put a small amount of Na into the hollow cathode, and measure the $\text{Na}(3^2P \rightarrow 3^2S)$ emission signal due to the electron excitation at energies from the threshold energy of 2.1 to 20 eV. The electron-excitation emission cross section of Na as a function of the energy is known.¹⁰ Thus the ratio of the electron-beam current within the viewing region at a low energy to the electron current at 20 eV is determined as being equal to the Na signal at a low energy divided by the signal at 20 eV times the Na excitation cross section at 20 eV divided by the cross section at the low energy. The electron currents through the viewing region at energies below 10 eV determined in this way typically differ from the current collected in the Faraday cup by 20% or less.

Figure 2 shows the optical emission cross sections for five transitions as functions of electron energy for electron excitation out of the 2^3S metastable level of He. The data are presented from threshold up to an energy of 16 eV. At higher energies the very small tail of the electron energy distribution may produce excitation of ground-level He atoms and cause the signal to rise, since the ground-level atoms have a much higher density than the metastable atoms. The apparent cross section for a particular level is equal to the sum of the cross sections for emission of light from that level to all lower levels. The optical cross section is equal to the apparent cross section times the known branching ratios.¹¹ Table I gives the absolute values of the apparent cross section (Q^A) at three different incident-electron energies along with the branching ratios used to convert the optical emission cross sections into the apparent cross sections. For the 5^3D and 6^3D levels, the optical cross sections are measured only at 10 eV because of the very low intensity

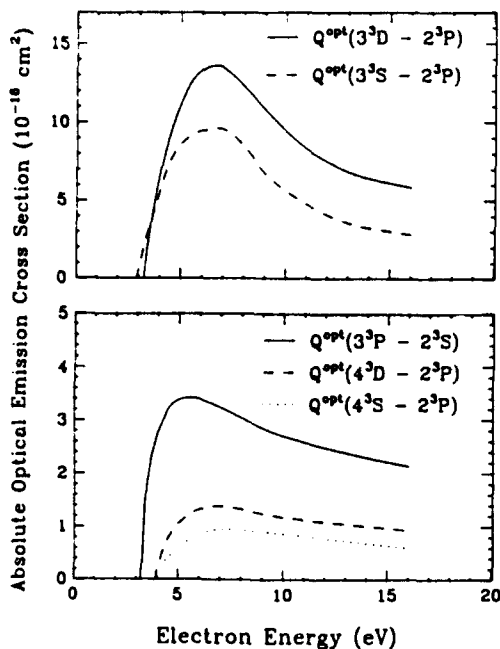


FIG. 2. Optical emission cross sections for five transitions as functions of electron energy for electron-impact excitation out of the 2^3S metastable level of He.

of the $5^3D \rightarrow 2^3P$ and $6^3D \rightarrow 2^3P$ transitions. The apparent excitation cross section is equal to the direct excitation cross section plus the cascade contribution. To use the optical cross section to obtain the direct cross section for exciting the 3^3P level from the 2^3S level, we determine the cascade contribution to 3^3P as follows. The optical emission cross sections for $n^3L \rightarrow 3^3P$ due to excitation out of the metastable level have not been measured, as the most important transitions are in the far infrared. However, we can determine the optical cross sections for $n^3L \rightarrow 3^3P$ from our measured optical cross sections for $n^3L \rightarrow 2^3P$ given in Fig. 2, since these two sets of cross sections are related by the ratios of the known Einstein A coefficients for the $n^3L \rightarrow 3^3P$ transitions to the known A coefficients for the $n^3L \rightarrow 2^3P$ transitions.¹¹ The direct cross section for exciting the 3^3P level from 2^3S at 4.5, 6.0, 10, and 16 eV are, respectively, 3.1×10^{-16} , 3.0×10^{-16} , 2.1×10^{-16} , and 1.7×10^{-16} cm^2 . Determination of the 3^3S direct cross section is handicapped by the lack of the $4^3P \rightarrow 2^3S$ optical-cross-section data. However, even if the $4^3P \rightarrow 2^3S$ optical cross section is as large as the $3^3P \rightarrow 2^3S$ cross section, the cascade from 4^3P to 3^3S is only 6% of the 3^3S apparent cross section at 10 eV. Thus we expect the 3^3S direct cross section to be at least 85% of the corresponding apparent cross section. A similar situation exists in the 3^3D cross section, although we have the additional uncertainty of the cascade from the n^3F levels. Nevertheless, from the relative magnitude of the apparent cross sections shown in Table I, it is clear that the direct cross section for 3^3P is smaller than those for 3^3S and 3^3D . This trend is different from the results of excitation

TABLE I. Apparent cross sections, $Q^A(n^3L)$, for electron excitation from the 2^3S to n^3L levels at incident-electron energies of 6, 10, and 16 eV. The apparent cross sections are equal to the measured optical emission cross sections divided by the branching ratios (BR) which are listed in the last column.

n^3L	$Q^A(n^3L)$ (10^{-16} cm^2)			BR
	6 eV	10 eV	16 eV	
3^3S	9.5	5.6	2.8	1.00
3^3P	3.8	3.0	2.3	0.90
3^3D	13	9.4	5.8	1.00
4^3S	1.5	1.5	1.0	0.59
4^3D	1.6	1.5	1.2	0.79
5^3D		0.24		0.72
6^3D		0.11		0.65

from the ground-state He atoms, where excitation to levels optically connected to the initial level has larger cross sections, but is in qualitative accord with theoretical calculations based on a Born-type approximation and on multichannel eikonal treatment.^{3,4} The latter³ gives *direct* cross sections of exciting 2^3S metastable atoms to the 3^3S , 3^3P , and 3^3D levels at 10 eV as, respectively, 1.51×10^{-16} , 0.615×10^{-16} , and 5.54×10^{-16} cm^2 , which are substantially smaller than our measured values. The 3^3S cross sections based on the Glauber approximation⁵ are mostly smaller than those of Ref. 3. More recently, Mathur *et al.*⁶ calculated direct excitation cross sections from the 2^3S to the 3^3S and 3^3P levels using a distorted-wave approximation. Their cross sections are larger than those of Ref. 3, but are still smaller than our measured values.

Gostev *et al.*¹ have reported measurements of cross sections for excitation of He atoms out of the 2^3S level to several higher levels at electron energies up to about 20 eV. Their measurements are made at higher density where secondary processes such as dissociative recombination make the interpretation of data difficult. Their 3^3P cross sections are in the same range of magnitude as ours, but their 3^3D and 4^3D cross sections are much larger than ours.

In conclusion, we have presented a novel method for measuring the electron cross sections for excitation out of a metastable level to another excited level. The method has been used to measure the excitation from the 2^3S level of He to seven other triplet levels. The uncertainty of the reported cross sections is estimated to be about 35%.

This work was supported in part by the Air Force Office of Scientific Research.

(a)Present address: PhotoMetrics, Inc., Woburn, MA 01801.

(b)Present address: Philips Lighting Company, Lynn, MA 01901.

¹V. A. Gostev, D. V. Elakhovskii, Yu. V. Zaitsev, L. A. Luizova, and A. D. Khakhaev, *Opt. Spektrosk.* **48**, 457 (1980) [*Opt. Spectrosc. (USSR)* **48**, 251 (1980)].

²M. R. Flannery, W. F. Morrison, and B. L. Richmond, *J. Appl. Phys.* **46**, 1186 (1975).

³M. R. Flannery and K. J. McCann, *Phys. Rev. A* **12**, 846 (1975).

⁴Y. K. Kim and M. Inokuti, *Phys. Rev.* **181**, 205 (1969).

⁵G. A. Khayrallah, S. T. Chen, and J. R. Rumble, Jr., *Phys. Rev. A* **17**, 513 (1978).

⁶K. C. Mathur, R. P. McEachran, L. A. Parcell, and A. D. Stauffer, *J. Phys. B* **20**, 1599 (1987).

⁷For a description of the optical method for measuring

electron-impact cross sections for excitation from the ground level, see A. R. Filippeli, S. Chung, and C. C. Lin, *Phys. Rev. A* **29**, 1709 (1984); M. B. Schulman, F. A. Sharpton, S. Chung, C. C. Lin, and L. W. Anderson, *Phys. Rev. A* **32**, 2100 (1985).

⁸R. M. St. John, F. L. Miller, and C. C. Lin, *Phys. Rev.* **134**, A888 (1964).

⁹D. W. Duquette, E. A. Den Hartog, and J. E. Lawler, *J. Quant. Spectrosc. Radiat. Transfer* **35**, 281 (1986).

¹⁰J. O. Phelps and C. C. Lin, *Phys. Rev. A* **24**, 1299 (1981).

¹¹W. L. Weise, M. W. Smith, and B. M. Glennon, *Atomic Transition Probabilities*, NBS, National Standards Reference Data Series—4 (U.S. GPO, Washington, DC, 1966), Vol. I.

Electron-impact excitation of the $x\ ^1\Sigma_g^-$, $y\ ^1\Pi_g$, and $o_3\ ^1\Pi_u$ Rydberg electronic states of the nitrogen molecule

James S. Allen, Sunggi Chung, and Chun C. Lin

Department of Physics, University of Wisconsin, Madison, Wisconsin 53706

(Received 8 September 1989; revised manuscript received 30 October 1989)

Electron-impact excitation of the $x\ ^1\Sigma_g^-$, $y\ ^1\Pi_g$, and $o_3\ ^1\Pi_u$ Rydberg electronic states of the nitrogen molecule has been studied. We have measured the maximum electron-impact optical-emission cross sections of many vibrational bands of the $y\ ^1\Pi_g \rightarrow w\ ^1\Delta_u$, $y\ ^1\Pi_g \rightarrow a'\ ^1\Sigma_u^-$, and $x\ ^1\Sigma_g^- \rightarrow a'\ ^1\Sigma_u^-$ electronic transitions. The maximum values of the optical-emission cross sections of these band systems are typically less than or on the order of 10^{-20} cm². The dependence of the emission cross sections of selected bands on electron energy has been studied. The excitation functions of the $y \rightarrow a'$ and $x \rightarrow a'$ bands have similar shapes below about 50 eV with a peak near 32 eV, and are approximately proportional to $1/E$ at high energies. We have measured the emission cross section of the $o_3\ ^1\Pi_u \rightarrow a\ ^1\Pi_g(0,0)$ band as a function of electron energy. The excitation function of the $o_3 \rightarrow a(0,0)$ band has a broader shape than the excitation functions of the $y \rightarrow w$, $y \rightarrow a'$, and $x \rightarrow a'$ bands. We have calculated Franck-Condon factors for the $y \rightarrow w$, $y \rightarrow a'$, and $x \rightarrow a'$ band systems and compare them with the experimental emission cross sections of these band systems. The apparent electron-impact-excitation cross sections of the vibrational levels of the x and y electronic states are estimated.

I. INTRODUCTION

The electron-impact excitation of the $x\ ^1\Sigma_g^-$, $y\ ^1\Pi_g$, and $o_3\ ^1\Pi_u$ Rydberg electronic states of the nitrogen molecule is investigated in the work reported here. The x , y , and o_3 states are the first (lowest-energy) terms of Rydberg series that converge to the $A\ ^2\Pi_u$ state of N_2^+ . The $v'=0$ vibrational levels of the x , y , and o_3 electronic states are, respectively, 14.04, 14.14, and 13.11 eV above the ground vibrational level of the $N_2\ X\ ^1\Sigma_g^+$ ground electronic state. The inner electrons of all three states have been assigned to the molecular-orbital (MO) configuration $(1\sigma_g)^2(1\sigma_u)^2(2\sigma_g)^2(2\sigma_u)^2(1\pi_u)^3(3\sigma_g)^2$, which is the MO configuration of the excited $N_2^+\ A\ ^2\Pi_u$ state. The outer electron of the x , y , and o_3 states is assigned to the Rydberg (R) $3p\pi_u$, $4p\sigma_u$, and $3s\sigma_g$ orbitals, respectively.¹ Inspection of the MO configurations of the electronic states of the nitrogen molecule listed in Ref. 1 reveals that transitions to the $a'\ ^1\Sigma_u^-$ and $o_3\ ^1\Pi_u$ electronic states are the only one-electron electric-dipole radiative decay channels from the x state. Likewise, for the y state we find four possible modes of one-electron electric-dipole emission: $y \rightarrow a'$, $y \rightarrow o_3$, $y \rightarrow w\ ^1\Delta_u$, and $y \rightarrow c_4'\ ^1\Sigma_u^+$. The valence states $a'\ ^1\Sigma_u^-$ and $w\ ^1\Delta_u$ have the same electron configuration, i.e., the $N_2^+\ A\ ^2\Pi_u$ core plus an outer $1\pi_g$ electron. The $o_3\ ^1\Pi_u$ state is optically connected to the ground electronic state, $X\ ^1\Sigma_g^+$, through the $3s\sigma_g \rightarrow 1\pi_u$ one-electron transition, whereas the $o_3\ ^1\Pi_u \rightarrow a\ ^1\Pi_g$ transition involves two active electrons. The x and y states are not optically connected to the ground state. The potential-energy curves of some of the above electronic states of N_2 are shown in Fig. 1. The potential-energy curves for the a' , o_3 , w , c_4' , and $a\ ^1\Pi_g$ states were taken from Ref. 1. The potential-energy

curves for the x and y states were calculated in this work (Sec. IV). The emission from the $x \rightarrow a'$ fifth positive, $y \rightarrow a'$ Kaplan first, $y \rightarrow w$ Kaplan second, and $o_3 \rightarrow a$ Gaydon-Herman band systems occurs in the ultraviolet region, between 2000 and 3100 Å.¹ The emission from the $x \rightarrow o_3$, $y \rightarrow o_3$, and $y \rightarrow c_4'$ band systems is in the infrared spectral region, and the $o_3 \rightarrow X$ emission occurs in the extreme ultraviolet spectral region. Electron-impact excitation of the x and y states could have a significant

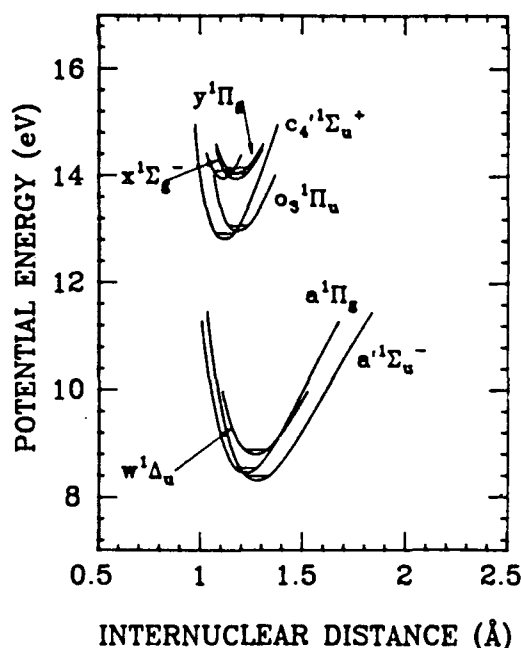


FIG. 1. Potential-energy curves for the $x\ ^1\Sigma_g^-$, $y\ ^1\Pi_g$, $o_3\ ^1\Pi_u$, $c_4'\ ^1\Sigma_u^+$, $w\ ^1\Delta_u$, $a'\ ^1\Sigma_u^-$, and $a\ ^1\Pi_g$ states of the N_2 molecule.

effect on the population of the long-living a' and w states through the $x \rightarrow a'$, $y \rightarrow a'$, and $y \rightarrow w$ band systems.

We are not aware of any measurements of the electron-impact optical-emission cross sections of the $x \rightarrow a'$, $y \rightarrow a'$, $y \rightarrow w$, or $o_3 \rightarrow a$ vibrational bands reported in the literature. These are weak band systems; however, the $x \rightarrow a'$ and $y \rightarrow w$ bands are relatively prominent features of the low-energy electron-impact-excitation spectrum of N_2 in the 2000–2800 Å region. The lifetimes of the $v'=1$ vibrational levels of the x and y electronic states, excited by electron impact, have been measured by Hummer and Burns.² They report values of 23.1 and 19.9 nsec, respectively, for the lifetimes of the x and y states. Electron-impact-excitation cross sections for the o_3 state have been determined by electron scattering experiments,^{3–5} and emission cross sections for the ultraviolet $o_3 \rightarrow X(0,0)$ and $(0,2)$ bands have been reported in Ref. 6.

In this paper we report the results of our study of electron-impact excitation of the $v'=0-2$ vibrational levels of the x and y electronic states and of the $v'=0$ level of the o_3 state. We have measured the maximum (peak) electron-impact optical-emission cross sections of many vibrational bands of the $x \rightarrow a'$, $y \rightarrow a'$, and $y \rightarrow w$ band systems and excitation functions for the x and y states. We have also obtained the emission cross section of the very weak $o_3 \rightarrow a(0,0)$ band. The experimental values of the optical-emission cross sections are compared with calculated values of the Franck-Condon factors of the band systems studied in this paper. Based on the emission cross sections reported in this paper, we have estimated the apparent electron-impact-excitation cross sections of the vibrational levels of the x and y states.

II. EXPERIMENT

The electron-impact optical-emission cross sections of the vibrational bands of the nitrogen band systems studied in this work have been measured using the apparatus and the procedure described in Refs. 7 and 8. In brief, an electron beam is formed inside a collision chamber filled with research grade N_2 gas at a pressure of 10 mTorr or less. The electron beam is collected by a Faraday cup, and the beam current is measured by an electrometer. The emission from a short segment of the electron beam is observed perpendicular to the beam axis through a slot in the wall of the Faraday cup and a window in the side of the collision chamber. The N_2 emission from the collision chamber passes through a scanning monochromator before being detected by a photomultiplier (EMI 9789QA). A circular stop defines the solid angle of the emission viewed by the monochromator, and the output current of the photomultiplier is measured with an electrometer and recorded on a chart recorder. A deuterium standard lamp, for which the spectral irradiance is known, is used for the absolute calibration of the N_2 emission signal. The N_2 gas pressure is measured with a capacitance manometer, and the N_2 number density is determined by the ideal-gas law, taking into account the local gas heating effect discussed in Ref. 7. The optical-emission cross sections for each vibrational band are

determined from the measured quantities in this experiment and Eq. (7) of Ref. 7. A diagram of the apparatus may be found in Ref. 8 and details of the experimental method in Ref. 7.

III. ANALYSIS AND RESULTS

A. $y\ ^1\Pi_g$ state

We have investigated electron-impact excitation of the $y\ ^1\Pi_g$ state by measuring the optical-emission cross sections of the vibrational bands of the $y \rightarrow w$ and $y \rightarrow a'$ band systems. The emission signals of many of the vibrational bands of the $y \rightarrow w$ and $y \rightarrow a'$ band systems are recorded in our spectral scans of the emission from the collision chamber. These bands are all overlapped to some extent by other N_2 emission bands. We have measured the maximum optical-emission cross sections of many of the $y \rightarrow w$ and $y \rightarrow a'$ bands, correcting for overlap by other N_2 emission bands using methods which will be described below. We have also studied the dependence of the $y \rightarrow w(1,3)$ and $(1,4)$ and $y \rightarrow a'(1,3)$ cross sections on electron energy and the dependence of the $y \rightarrow w(1,3)$ emission signal on N_2 pressure and electron beam current.

The absolute values of the maximum optical-emission cross sections determined in this work and the estimated uncertainties of these values are listed in Table I. The maximum values of the $y \rightarrow w$ and $y \rightarrow a'$ cross sections are typically less than or on the order of 10^{-20} cm². The absolute value of the $y \rightarrow w(1,3)$ maximum cross section was measured at static N_2 pressures of less than 10 mTorr, where the linear relation between the observed emission signal and the gas pressure is confirmed experimentally, as described in the last paragraph of Sec. III A. The remainder of the $y \rightarrow w$ and $y \rightarrow a'$ cross sections were measured relative to the cross section of the $y \rightarrow w(1,3)$ band and the cross sections of the $N_2\ D\ ^3\Sigma_u^+ \rightarrow B\ ^3\Pi_g(0,1)$ and $(0,4)$ bands with N_2 gas flowing through the collision chamber at pressures of less than 10 mTorr. Flowing the N_2 gas through the collision chamber eliminates the accumulation of contaminating species inside the collision chamber. The relative cross sections were then normalized to the absolute value of the $y \rightarrow w(1,3)$ cross section determined in this work, and to the absolute values of the $D \rightarrow B(0,1)$ and $(0,4)$ cross sections reported in Ref. 7. The $D \rightarrow B(0,1)$ and $(0,4)$ emission is stronger and can be measured with a lower uncertainty than the $y \rightarrow w(1,3)$ emission, and the $D \rightarrow B$ bands are located in the same wavelength region as the $y \rightarrow w$ and $y \rightarrow a'$ bands studied in this work. Therefore the $D \rightarrow B(0,1)$ and $(0,4)$ band cross sections reported in Ref. 7 provide a convenient standard to which the relative values of the $y \rightarrow w$ and $y \rightarrow a'$ cross sections determined in this experiment can be normalized. We have determined the values of the cross sections of selected $y \rightarrow w$ and $y \rightarrow a'$ bands by normalization to the $D \rightarrow B(0,0)$ and $(0,4)$ cross sections and by normalization to the absolute value of the $y \rightarrow w(1,3)$ cross section, and the two sets of cross sections are found to be identical within the experimental uncertainty.

TABLE I. Comparison of the experimental maximum (peak) optical-emission cross sections for the (v', v'') bands of the $y \rightarrow w$, $y \rightarrow a'$, and $x \rightarrow a'$ transitions with two sets of Franck-Condon (FC) cross sections obtained by the Morse potentials and by the RKR potentials of the x and y states. The third column shows the method of correction (MC) used to subtract the signal due to overlapping bands. The estimated percentage uncertainties of the experimental cross sections are listed under "% uncertainty." Those experimental cross sections marked with an asterisk are used to normalize the FC cross sections.

Band	λ (Å)	MC ^a	% uncertainty	Cross section (10^{-21} cm ²)		
				Expt.	Morse	RKR
$y \rightarrow w(0,0)$	2355	B	73	3.6	6.3	5.3
	(0,1)	C	92	7.4	6.6	6.1
	(0,2)	A	25	3.6*	4.3	4.3
	(0,3)	A	30	2.6*	2.2	2.3
	(0,4)				0.94	1.0
	(0,5)	B	67	0.4	0.36	0.40
	(0,6)				0.12	0.15
$y \rightarrow w(1,0)$	2263	C	20	27.8	26.2	25.5
	(1,1)				1.4	2.9
	(1,2)	A	38	1.6	2.2	1.1
	(1,3)	A	23	5.8*	6.0	5.5
	(1,4)	B	33	5.9*	5.7	6.3
	(1,5)	A	21	4.7	3.6	4.5
	(1,6)	A	29	2.4	1.9	2.6
	(2,0)	A	36	5.8*	5.8	5.8
	(2,1)				3.8	1.7
	(2,2)				2.4	2.7
	(2,3)				0.03	0.39
	(2,4)				<0.2	0.14
	(2,5)	B	87	0.7	1.3	0.85
	(2,6)	A	37	0.5	1.3	1.1
	$y \rightarrow a'(0,0)$	2154	A	31	5.2*	5.2
(0,1)		B	97	3.7	6.4	7.0
(0,2)		N		<9.0	4.8	5.5
(0,3)					2.8	3.3
(0,4)		N		<3.2	1.4	1.7
$y \rightarrow a'(1,0)$	2077	N		<19.0	21.0	24.3
	(1,1)				2.9	5.5
	(1,2)			<0.4	0.57	0.14
	(1,3)	A	32	3.8*	3.8	3.8
	(1,4)	A	42	2.1	4.8	6.0
	(2,6)	N		<1.2	<0.24	<0.19
	(2,7)			<0.2*	<0.20	<0.20
	(2,8)				<0.13	<0.16
$x \rightarrow a'(0,0)$	2199				<2.1	<2.1
	(0,1)	N		<3.9*	<3.0	<3.0
	(0,2)				<2.5	<2.5
	(0,3)				<1.6	<1.6
	(0,4)	N		<0.6*	<0.84	<0.85
	(0,5)				<0.40	<0.41
	(0,6)				<0.18	<0.18
	(0,7)				<0.07	<0.07
	(0,8)				<0.03	<0.03
	(0,9)				<0.01	<0.01
$x \rightarrow a'(1,0)$	2112	N		<73.0	32.6	31.9
	(1,1)	N		<16.2	9.1	9.1
	(1,2)				0.02	0.01
	(1,3)	N		<8.4	4.3	4.2
	(1,4)	N		<7.0	7.7	7.6

TABLE I. (Continued).

Band	λ (Å)	MC ^a	% uncertainty	Cross section (10^{-21} cm ²)		
				Expt.	Morse	RKR
$x \rightarrow a'(1,5)$	2497	<i>N</i>		< 7.6	7.2	7.2
(1,6)	2587	<i>B</i>	27	4.9*	5.0	5.0
(1,7)	2682	<i>B</i>	26	3.0*	2.9	2.9
(1,8)	2782	<i>A</i>	35	1.6	1.5	1.5
(1,9)	2888				0.72	0.72
(1,10)	3001				0.32	0.33
$x \rightarrow a'(2,0)$	2034	<i>A</i>	22	28.6*	28.6	28.6
(2,1)	2098	<i>A</i>	59	3.3	2.0	1.8
(2,2)	2165	<i>A</i>	57	8.8 ^b	12.1	11.9
(2,3)	2236	<i>N</i>		< 16.0	5.0	5.1
(2,4)	2310				0.07	0.07
(2,5)	2388	<i>N</i>		< 8.7	1.7	1.6
(2,6)	2470	<i>N</i>		< 10.5	4.1	4.0
(2,7)	2556	<i>N</i>		< 5.1	4.5	4.5
(2,8)	2647	<i>A</i>	31	2.0	3.6	3.6
(2,9)	2743	<i>B</i>	45	2.5	2.4	2.4
(2,10)	2845	<i>A</i>	32	1.5	1.4	1.4

^aMethods *A*, *B*, and *C* are explained in Sec. III A. An *N* in this column means no correction is made for this particular band.

^bThe emission cross section of the $a \rightarrow X(7,16)$ band, which overlaps the $x \rightarrow a'(2,2)$ band, is assumed to be negligible in comparison with the cross section of the $x \rightarrow a'(2,2)$ band. See Sec. III B.

Since the $y \rightarrow w(0, v'')$ bands with $v''=2,3,5$, the $y \rightarrow w(1, v'')$ bands with $v''=3,4,5$, the $y \rightarrow w(2,0)$ and $(2,4)$ bands, the $y \rightarrow a'(0, v'')$ bands with $v''=0,1,4$, and the $y \rightarrow a'(1,4)$ and $(2,6)$ bands are contaminated by bands of the $N_2^+ D^2\Pi_g \rightarrow A^2\Pi_u$ band system, the relative cross sections of these bands were measured at an electron energy of 20.0 eV in order to eliminate contamination by the $N_2^+ D^2\Pi_g \rightarrow A^2\Pi_u$ band system which has an excitation onset of 22.0 eV.¹ The peak values of the cross sections were determined by multiplying the cross sections at 20.0 eV by the ratio of the value of the $y \rightarrow w(1,3)$ cross section at its peak (at 32 eV) to its value at 20.0 eV. The cross sections of those $y \rightarrow w$ and $y \rightarrow a'$ bands that are not overlapped by any of the $N_2^+ D \rightarrow A$ bands were measured at 32 eV.

The $y \rightarrow w$ and $y \rightarrow a'$ cross sections listed in Table I have been corrected for contamination by other N_2 bands by three different methods depending on the extent of the contamination. The method used to correct each band for contamination is indicated as method *A*, *B*, or *C* in Table I. Each method is described below. The cross sections labeled with an *N* in Table I include the contributions of other N_2 bands; we were unable to correct the emission signal of these bands for contamination.

The primary method, method *A*, of correcting the emission cross sections for contamination is based entirely on our spectral scans, and it is applicable to those $y \rightarrow w$ and $y \rightarrow a'$ bands which are overlapped by, but sufficiently resolved from, adjacent N_2 bands in our spectral scans of the emission signal as a function of wave-

length. The emission signal of a $y \rightarrow w$ band in the above category, for example, is determined by linearly extrapolating the signal versus wavelength curve of the $y \rightarrow w$ band from a wavelength region of the scan in which the $y \rightarrow w$ band is free of contamination into the wavelength region of the scan where it overlaps the adjacent N_2 band. The area bounded by the uncontaminated and extrapolated portions of the signal versus wavelength curve of the $y \rightarrow w$ band and by the background signal level (the signal observed in a nearby wavelength region which does not contain any N_2 emission bands) is then measured to obtain the emission signal of the $y \rightarrow w$ band. In an alternative approach, the signal versus wavelength curve of the adjacent N_2 band is linearly extrapolated from a wavelength region of the scan in which the emission signal of the adjacent N_2 band is dominant into the region where it overlaps the $y \rightarrow w$ band. In this approach the area bounded by the signal versus wavelength curve of the combined $y \rightarrow w$ band and overlapping portion of the adjacent N_2 band, the extrapolated portion of the signal versus wavelength curve of the adjacent band, and the background signal level is measured to obtain the emission signal of the $y \rightarrow w$ band. The first approach is used when the adjacent N_2 band is violet-degraded with a bandhead wavelength at a shorter wavelength than the bandhead wavelength of the $y \rightarrow w$ band or when the $y \rightarrow w$ band emission is much stronger than the adjacent N_2 band. The second approach is used when the adjacent N_2 band is violet-degraded with a bandhead wavelength at a longer wavelength than the bandhead wavelength of

the $y \rightarrow w$ band or when the adjacent N_2 band emission is much stronger than the $y \rightarrow w$ emission. If the adjacent N_2 band is red-degraded with a bandhead wavelength at a shorter wavelength than the bandhead wavelength of the $y \rightarrow w$ band, we use either the first or the second approach, depending upon whether the $y \rightarrow w$ band emission or the adjacent N_2 band emission appears to be stronger. The $y \rightarrow w$ and $y \rightarrow a'$ bands are all violet-degraded bands. The uncertainty in the cross sections obtained by method *A* depends on the degree of overlap between the two bands and the relative intensities of the two bands.

Another method, method *B*, which uses Franck-Condon factors to estimate the extent of the contamination, is adopted in cases where the $y \rightarrow w$ or $y \rightarrow a'$ band is not resolved from the contaminating N_2 band in our special scans. In the Franck-Condon approximation, the ratio of the emission cross sections, $Q(\alpha v_i' \rightarrow \beta v_j'')$ and $Q(\alpha v_i' \rightarrow \beta v_k'')$, of two vibrational bands of a given band system, $\alpha \rightarrow \beta$, with the same initial state v_i' is approximately given by

$$\frac{Q(\alpha v_i' \rightarrow \beta v_j'')}{Q(\alpha v_i' \rightarrow \beta v_k'')} \approx \left[\frac{\lambda(\alpha v_i' \rightarrow \beta v_k'')}{\lambda(\alpha v_i' \rightarrow \beta v_j'')} \right]^3 \frac{q(\alpha v_i' \rightarrow \beta v_j'')}{q(\alpha v_i' \rightarrow \beta v_k'')} \quad (1)$$

where $q(\alpha v_i' \rightarrow \beta v_j'')$ is the Franck-Condon factor and $\lambda(\alpha v_i' \rightarrow \beta v_j'')$ is the wavelength of the $\alpha \rightarrow \beta(v_i', v_j'')$ band. In method *B*, in order to correct for the contamination of a $y \rightarrow w(v_i', v_j'')$ band by a band $\alpha \rightarrow \beta(v_i', v_j'')$, we calculate the Franck-Condon factors for the $\alpha \rightarrow \beta$ band system, measure the emission cross section of a different band of the $\alpha \rightarrow \beta$ system, (v_i', v_k'') , that is not seriously contaminated by other bands, and use Eq. (1) to determine the cross section of the $\alpha \rightarrow \beta(v_i', v_j'')$ band. The emission cross section of the combined $y \rightarrow w(v_i', v_j'')$ and $\alpha \rightarrow \beta(v_i', v_j'')$ bands is measured, correcting for overlap by adjacent N_2 bands using method *A* above when necessary. The estimated value of the $\alpha \rightarrow \beta(v_i', v_j'')$ cross section is then subtracted from the cross section of the combined bands. The accuracy of Eq. (1) varies from one case to another. Unless otherwise noted below, for the purpose of error estimation, we assign a 35% uncertainty to Eq. (1), so that the estimated uncertainty of $Q(\alpha v_i' \rightarrow \beta v_j'')$ is taken as the quadrature sum of the uncertainty of the measured $Q(\alpha v_i' \rightarrow \beta v_k'')$ and the 35% uncertainty of Eq. (1).

A third method, method *C*, is exemplified by the $y \rightarrow w(1,0)$ band, which is severely contaminated by the $N_2 D^3\Sigma_u^- \rightarrow B^3\Pi_g(0,0)$ band. The value of the $y \rightarrow w(1,0)$ cross section listed in Table I was obtained by the following procedure. We measured the emission cross section of the combined $y \rightarrow w(1,0)$ and $D \rightarrow B(0,0)$ bands at 32 eV. Since the excitation function for the $D \rightarrow B$ emission peaks at 14.1 eV which is just below the appearance potential of the $y \rightarrow w(1,0)$ band, we can measure the cross section of the $D \rightarrow B(0,0)$ band alone at 14.1 eV. The value of the $D \rightarrow B(0,0)$ emission cross section at 32 eV is then obtained by using the shape of the excitation function of the $D \rightarrow B(0,1)$ band reported in Ref. 7 to scale the measured cross section of the $D \rightarrow B(0,0)$ band at 14.1 eV. We subtracted this value of

the $D \rightarrow B(0,0)$ emission cross section at 32 eV from the emission cross section of the combined $y \rightarrow w(1,0)$ and $D \rightarrow B(0,0)$ bands at 32 eV to obtain the $y \rightarrow w(1,0)$ emission cross section at 32 eV.

The estimated uncertainty of 23% in the absolute value of the $y \rightarrow w(1,3)$ maximum cross section listed in Table I was determined by adding in quadrature the estimated uncertainty of each of the quantities in Eq. (7) of Ref. 7. In particular, this value of the uncertainty includes estimated uncertainties in the measured $y \rightarrow w(1,3)$ emission signal of 10% due to the uncertainty in the correction for overlap, using method *A*, by the $k \rightarrow w(1,3)$ and $c_3^1\Pi_u \rightarrow a^1\Pi_g(2,0)$ bands, 3% due to the uncertainty in the background signal level, and 5% due to the signal noise in our spectral scans of this band.

The estimated uncertainties in the maximum cross sections of each of the remaining $y \rightarrow w$ and $y \rightarrow a'$ bands listed in Table I allow for the estimated uncertainty in our experimental values for the relative wavelength response of the optical system (4–7%, depending on the wavelength), the uncertainty in the value of the maximum $D \rightarrow B(0,1)$ cross section reported in Ref. 7 (8%), and the uncertainty in the measured emission signals of the $y \rightarrow w$ or $y \rightarrow a'$ bands relative to the $D \rightarrow B(0,1)$ emission signal. The estimated uncertainties in the cross sections of those bands which were measured at 20 eV and then converted to peak values include an additional 13% uncertainty in the ratio of the maximum value of the $y \rightarrow w(1,3)$ cross section to its value at 20 eV. The uncertainty in the measured emission signal includes the uncertainty due to the corrections made for contamination by other N_2 bands using methods *A*, *B*, or *C*, the uncertainty due to the correction for the background signal, and the uncertainty due to signal noise. The uncertainty in the emission cross section varies from band to band depending on the extent of the contamination and the strength of the signal and is listed in Table I.

The peak values of the $y \rightarrow w(0,2)$, (0,3), (1,2), (1,3), (1,5), (1,6), (2,0), and (2,6), and $y \rightarrow a'(0,0)$, (1,3), and (1,4) emission cross sections listed in Table I have been corrected for overlap by adjacent N_2 bands using method *A*. The uncertainty due to the correction for overlap, using method *A*, varies from 3% to 30%. The uncertainties due to the correction for background and due to signal noise vary from less than 5% for the stronger emission bands to about 15% for the weakest emission bands. The correction for the $y \rightarrow w(0,2)$ band entails a consideration of the energy dependence of the emission signal of this band. In order to avoid disrupting the continuity of the presentation, we describe the analysis for the $y \rightarrow w(0,2)$ band in the Appendix.

The peak values of the $y \rightarrow w(0,0)$, (1,4), (0,5), (2,5), and $y \rightarrow a'(0,1)$ cross sections have been corrected for contamination using method *B*. The peak cross sections of the $y \rightarrow w(0,0)$ and (1,4) bands have been corrected for contamination by the $x \rightarrow a'(0,2)$ and (0,5) bands, respectively, based on our calculated values of the Franck-Condon factors for the $x \rightarrow a'$ band system (Sec. IV) and our experimental limits for the emission cross sections of the $x \rightarrow a'(0,1)$ and (0,4) bands (Sec. III B). The magnitude of the correction to the $y \rightarrow w(1,4)$ cross section is

about 6% of the combined $y \rightarrow w(1,4)$ and $x \rightarrow a'(0,5)$ cross section. The correction to the $y \rightarrow w(0,0)$ cross section is much larger, about 29% of the combined $y \rightarrow w(0,0)$ and $x \rightarrow a'(0,2)$ cross section. Similarly, the $y \rightarrow w(0,5)$ cross section has been corrected for contamination by the $o_3 \rightarrow a(0,1)$ band using calculated Franck-Condon factors for the $o_3 \rightarrow a$ band system (Sec. III C) and our experimental limit for the $o_3 \rightarrow a(0,0)$ cross section (Sec. III C). The magnitude of this correction is about 20% of the combined $y \rightarrow w(0,5)$ and $o_3 \rightarrow a(0,1)$ cross section. The $y \rightarrow w(2,5)$ cross section has been corrected for contamination of the $y \rightarrow a'(2,8)$ band based on calculated Franck-Condon factors for the $y \rightarrow a'$ band system (Sec. IV) and the experimental limit for the $y \rightarrow a'(2,7)$ cross section listed in Table I. We estimate the value of this correction to be about 21% of the combined $y \rightarrow w(2,5)$ and $y \rightarrow a'(2,8)$ cross section. The $y \rightarrow a'(0,1)$ cross section has been corrected for contamination by the $c_4^1\Pi_u \rightarrow a^1\Pi_g(0,1)$ band based on our calculated Franck-Condon factors for the $c_4 \rightarrow a$ band system and our experimental values of the $c_4 \rightarrow a(0,2)$ and $(0,4)$ emission cross sections. The $c_4 \rightarrow a$ Franck-Condon factors were calculated using the Rydberg-Klein-Rees (RKR) potential for the a state given in Ref. 1 and a Morse potential for the c_4 state based on the molecular constants for the c_4 state given in Ref. 9. We estimate that the $c_4 \rightarrow a(0,1)$ band accounts for 52% of the combined $y \rightarrow a'(0,1)$ and $c_4 \rightarrow a(0,1)$ signal at 32 eV. The estimated uncertainties in the maximum values of the $y \rightarrow w(0,0)$, $(0,5)$, $(1,4)$, and $(2,5)$, and $y \rightarrow a'(0,1)$ cross sections due to the above corrections are 40%, 25%, 9%, 32%, and 67%, respectively, whereas the corresponding overall uncertainties are 73%, 67%, 33%, 87%, and 97%, as shown in Table I.

Method C is applied to the $y \rightarrow w(1,0)$ and $(0,1)$ bands to correct for contamination by the $N_2 D^3\Sigma_u^+ \rightarrow B^3\Pi_g(0,0)$ and $(0,2)$ bands, respectively. The $D \rightarrow B(0,0)$ band accounts for 38% of the combined $y \rightarrow w(1,0)$ and $D \rightarrow B(0,0)$ signal at 32 eV, whereas 78% of the combined $y \rightarrow w(0,1)$ and $D \rightarrow B(0,2)$ signal at 32 eV is due to the $D \rightarrow B(0,2)$ band. The portions of the error in the $y \rightarrow w(1,0)$ and $(0,1)$ cross sections listed in Table I due to this correction procedure are 6% and 90%, respectively.

The upper limits of the $y \rightarrow a'(0,2)$, $(0,4)$, $(1,0)$, and $(2,6)$ cross sections listed in Table I include contributions from other N_2 bands. The $(0,2)$ band is contaminated by the $A^3\Sigma_u^+ \rightarrow X^1\Sigma_g^-(2,4)$ and $a^1\Pi_g \rightarrow X^1\Sigma_g^+(4,15)$ bands, the $(0,4)$ band is contaminated by the $A \rightarrow X(0,4)$ and $a \rightarrow X(13,24)$ bands, the $(1,0)$ band is contaminated by the $a \rightarrow X(2,11)$ band, and the $(2,6)$ band is contaminated by the $a \rightarrow X(11,22)$, $k^1\Pi_g \rightarrow w^1\Delta_u(1,2)$ bands, and possibly by the $A \rightarrow X(2,5)$ band. However, as discussed later on in this paper (Secs. III B and III C), the emission signals of the $A \rightarrow X$ bands are probably too weak to influence the observed emission signals of the band systems studied in this paper. Since we did not observe any $a \rightarrow X(v',v'')$ bands with $v'=2, 4, 11$, or 13 that were sufficiently free of contamination by other N_2 bands, we were not able to correct the $y \rightarrow a'(0,2)$, $(0,4)$, $(1,0)$, or $(2,6)$ bands for $a \rightarrow X$ contamination using

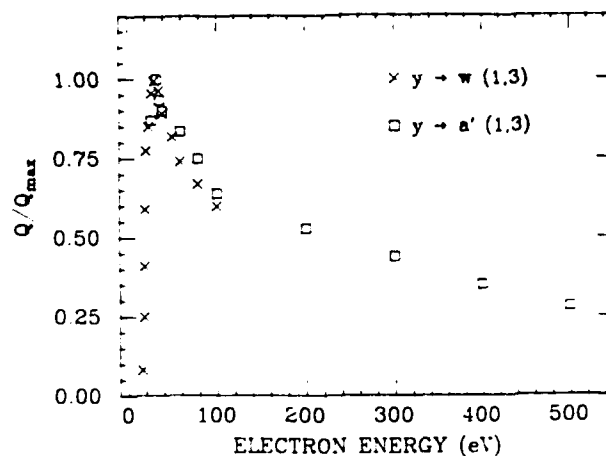


FIG. 2. Ratio of the optical-emission cross section Q to its peak value Q_{\max} as a function of the incident electron energy (excitation function) for the $y \rightarrow a'(1,3)$ band (\square) and the $y \rightarrow w(1,3)$ band (\times).

method B. For these bands we enter the symbol N in the third column of Table I to indicate that no correction for overlap is made. The emission signal in the wavelength regions corresponding to the locations of the $y \rightarrow w(2,4)$ and the $y \rightarrow a'(1,2)$ and $(2,7)$ bands is comparable to the level of the background signal, therefore we list only upper limits for the cross sections of these bands. The $y \rightarrow w(0,6)$, $(1,1)$, $(2,1)$, $(2,2)$, $(2,3)$, and the $y \rightarrow a'(0,3)$, $(1,1)$, and $(2,8)$ bands were masked by other emission bands of N_2 , therefore we do not report emission cross sections for these bands.

The dependence of the $y \rightarrow a'(1,3)$ optical-emission cross section on incident electron energy for energies up to 500 eV, determined in this work, is shown in Fig. 2. The excitation function peaks at 32 eV and is roughly proportional to $1/E$ above 300 eV. Below 100 eV the shape of our measured excitation function of the $y \rightarrow w(1,3)$ signal is identical to that of the $y \rightarrow a'(1,3)$ band, but the values of Q/Q_{\max} for the $y \rightarrow w(1,3)$ band are larger than the corresponding values of Q/Q_{\max} for the $y \rightarrow a'(1,3)$ band by less than 5% between 200 and 400 eV. This is because the $y \rightarrow w(1,3)$ band is contaminated by the $N_2^+ D^2\Pi_g \rightarrow A^2\Pi_u(3,3)$ band. The excitation function for the latter has a broad peak at about 200 eV, thus the influence of the N_2^+ band contamination is more noticeable at high energies. We have also checked the dependence of the $y \rightarrow w(1,4)$ emission cross section on electron energy and we find that the excitation function of this band is in agreement with the excitation function for the $y \rightarrow a'(1,3)$ band within the experimental uncertainty of our measurements. The estimated uncertainty in the values of the $y \rightarrow w(1,3)$ emission cross sections relative to the peak value is less than 15% below 100 eV. The estimated uncertainty in the relative values of the $y \rightarrow a'(1,3)$ emission cross sections is about 15% below 100 eV and about 20% above 100 eV.

We have investigated the N_2 pressure and electron beam current dependence and the polarization of the $y \rightarrow w(1,3)$ emission signal. We have measured the pres-

sure dependence of the $y \rightarrow w(1,3)$ emission at electron energies of 20, 32, and 150 eV and we find that the emission signal depends linearly on pressure in the 1–10 mTorr pressure range at each energy. We have also checked the dependence of the emission signal, at 32 eV, on N_2 pressure (up to 11 mTorr) of the $y \rightarrow w(0,2)$, (0,3), (1,2), (1,5), (1,6), (2,0), and (2,6) bands, and of the $y \rightarrow a'(1,3)$ band. We find that the emission signals of all of the above bands depend linearly on pressure. We measured the dependence of the $y \rightarrow w(1,3)$ emission on electron beam current at 32 eV over a range of beam currents from 50 to 400 μA and we find that the signal depends linearly on the beam current over this range. The $y \rightarrow w$ and $y \rightarrow a'$ cross sections reported in this paper were measured with beam currents of less than 350 μA . We have also measured the polarization of the $y \rightarrow w(1,3)$ emission at 32 eV and we find that the polarization is very small ($P \approx -0.02$), therefore the polarization correction to the emission cross sections is negligible.

B. $x \ ^1\Sigma_g^-$ state

The production of N_2 molecules in the $v'=0,1,2$ levels of the $x \ ^1\Sigma_g^-$ state by electron impact has been investigated by studying the fifth positive ($x \rightarrow a'$) band system emission from the collision chamber. We have measured the maximum optical-emission cross sections of several $x \rightarrow a'$ vibrational bands, correcting for overlap by other N_2 emission bands using methods *A* or *B* described above. The energy dependence of the $x \rightarrow a'(2,0)$ and (1,7) optical-emission cross sections and the dependence of the $x \rightarrow a'(1,7)$ emission signal on N_2 pressure and on electron beam current have also been investigated.

The maximum values of the $x \rightarrow a'$ optical-emission cross sections determined in this work and the estimated uncertainties of these values are listed in Table I. Those cross sections which were corrected for contamination using methods *A* or *B* are labeled with an *A* or *B*, respectively. The cross sections of all of the $x \rightarrow a'$ bands, with the exception of the (1,4), (1,6), (2,6), (2,8), and (2,10) bands, were measured at an electron energy of 32 eV, which corresponds to the peak in the $x \rightarrow a'(1,7)$ and (2,0) excitation functions. The cross sections of the (1,4), (1,6), (2,6), (2,8), and (2,10) bands were measured at 20.0 eV to eliminate contamination by $N_2 \ ^D \rightarrow A$ bands and were converted to peak values using the excitation function of the $x \rightarrow a'(1,7)$ band.

The $x \rightarrow a'(1,8)$, (2,0), (2,1), (2,8), and (2,10) emission cross sections have been corrected for overlap by adjacent N_2 bands using method *A*. The uncertainty in the maximum values of the cross sections due to the correction for overlap varies from 3% to 30% for these bands.

The $x \rightarrow a'(1,6)$, (2,2), (1,7), and (2,9) peak cross sections have been corrected for contamination by other N_2 bands using method *B*. The cross section of the (1,6) band has been corrected for contamination by the $a \rightarrow X(14,26)$ band using the Franck-Condon factors for the $a \rightarrow X$ band system and our experimental upper limit for the $a \rightarrow X(14,25)$ cross section. The $a \rightarrow X$ Franck-Condon factors were calculated using the RKR potentials for the a and X states given in Ref. 1. We note that

Holland¹⁰ found reasonably good agreement between his experimentally determined $a \rightarrow X$ cross sections and the $a \rightarrow X$ Franck-Condon factors from Ref. 11. Our values for the Franck-Condon factors of the $a \rightarrow X$ bands are in good agreement with the corresponding values reported in Ref. 11. Therefore we have assigned an uncertainty of 20% to Eq. (1) for the purpose of estimating the uncertainty of the $a \rightarrow X(14,26)$ cross section. The $a \rightarrow X(14,26)$ cross section obtained above is less than 8% of the maximum $x \rightarrow a'(1,6)$ cross section, therefore this is a very minor correction. Similarly, we attempt to correct the $x \rightarrow a'(2,2)$ emission for contamination by the $a \rightarrow X(7,16)$ band using the $a \rightarrow X(7,19)$ cross section along with the appropriate Franck-Condon factors. The $a \rightarrow X(7,19)$ emission, however, is not distinguishable from the background signal in our spectral scans, thus we can only assign an upper limit of 1.5×10^{-22} cm² for the $a \rightarrow X(7,19)$ cross section at 32 eV. Taking this upper limit as the value of the $a \rightarrow X(7,19)$ cross section we find that the $a \rightarrow X(7,16)$ band accounts for 57% of the combined $x \rightarrow a'(2,2)$ and $a \rightarrow X(7,16)$ signal at 32 eV. In other words, the correction due to the $a \rightarrow X(7,16)$ contamination may be anywhere between 0% and 57% of the observed signal. Ajello and Shemansky¹² indicated that they did not detect $a \rightarrow X(v',v'')$ emission from the $v'=7, 8$, and 9 vibrational levels excited by electron impact on N_2 . They suggest that the $a \ ^1\Pi_g$ state is 100% predissociated for $v' \geq 7$. In the absence of a quantitative determination of the $a \rightarrow X(7,16)$ cross section, we adopt the suggestion of Ajello and Shemansky and neglect the $a \rightarrow X(7,16)$ contribution to our observed signal. However, we must point out that even with predissociation it is possible to have some $a \rightarrow X(7,v'')$ emission. For instance, even for a value of the $a \rightarrow X(7,19)$ cross section as small as 0.3×10^{-22} cm², method *B* predicts a 10% contribution of the $a \rightarrow X(7,16)$ band to the combined signal of the $x \rightarrow a'(2,2)$ and $a \rightarrow X(7,16)$ bands. Thus the value of the $x \rightarrow a'(2,2)$ cross section listed in Table I, which is obtained by neglecting the $a \rightarrow X(7,16)$ contamination, may be slightly larger than the true value. More refined measurements are needed to settle this issue. The $x \rightarrow a'(2,2)$ cross section has not been corrected for contamination by the $A \rightarrow X(4,4)$ band; however, the $A \ ^3\Sigma_u^+$ state is a metastable state (the radiative lifetime of the $v'=0$ level of the $A \ ^3\Sigma_u^+$ state is 1.9 s),¹ therefore the $A \rightarrow X(4,4)$ band most probably does not make a significant contribution to the observed emission signal. If the radiative lifetime of the $v'=4$ level of the *A* state is comparable to that of the $v'=0$ level, then, in our experiment, most of the N_2 molecules in the $v'=4$ level will collide with the Faraday cup, electron gun grids, or the walls of the collision chamber before emitting a photon in the $A \rightarrow X(4,4)$ transition. The maximum cross section of the $x \rightarrow a'(1,7)$ band has been corrected for contamination by the $c'_4 \rightarrow a(4,4)$ band using our calculated values of the Franck-Condon factors for the $c'_4 \rightarrow a$ band system and the values of the $c'_4 \rightarrow a(4,0)$ and (4,1) cross sections and excitation functions reported in Ref. 8. The experimental value of the ratio of the $c'_4 \rightarrow a(4,0)$ and (4,1) emission cross sections differs from the value predicted by Eq. (1) by about 45%; therefore, we have as-

signed an uncertainty of 45% to Eq. (1) in this case. We estimate that the $c'_4 \rightarrow a(4,4)$ band accounts for less than 8% of the combined $x \rightarrow a'(1,7)$ and $c'_4 \rightarrow a(4,4)$ emission signal at 32 eV. The cross section of the $x \rightarrow a'(2,9)$ band has been corrected for contamination by the $y \rightarrow w(0,4)$ band using our calculated values of the Franck-Condon factors for the $y \rightarrow w$ band system (Sec. IV) and the values of the $y \rightarrow w(0,2)$ and $(0,3)$ cross sections listed in Table I. We find that the emission cross sections of the $y \rightarrow w(0, v'')$ bands calculated using Eq. (1) agree with the corresponding experimental values of the $y \rightarrow w(0, v'')$ emission cross sections within 35%. The $y \rightarrow w(0,4)$ band accounts for 24% of the combined $x \rightarrow a'(2,9)$ and $y \rightarrow w(0,4)$ signal at 32 eV. We estimate that the uncertainties in the peak values of the $x \rightarrow a'(1,6)$, $(1,7)$, and $(2,9)$ cross sections due to the above corrections are about 5%, 6%, and 21%, respectively.

The upper limits of the $x \rightarrow a'(0,1)$, $(0,4)$, $(1,0)$, $(1,1)$, $(1,3)$, $(1,4)$, $(1,5)$, $(2,3)$, $(2,5)$, $(2,6)$, and $(2,7)$ cross sections listed in Table I include the contributions of other N_2 bands. The $(0,1)$ band is contaminated by the $a \rightarrow X(8,18)$, $A \rightarrow X(4,5)$, and $E^3\Sigma_g^+ \rightarrow A^3\Sigma_u^+(1,3)$ bands, and the $(0,4)$ band is contaminated by the $A \rightarrow X(4,7)$ and $c'_4 \rightarrow a(2,0)$ bands. The $(1,0)$, $(1,1)$, and $(2,3)$ bands are severely overlapped by the $a \rightarrow X(4,13)$, $(3,13)$, and $(6,16)$ bands, respectively. The $(1,3)$ band is contaminated by the $a \rightarrow X(11,21)$ and $k^1\Pi_g \rightarrow a^1\Sigma_u^-(0,2)$ bands, the $(1,4)$ band by the $k \rightarrow a'(0,3)$ band, and the $(1,5)$ band by the $E \rightarrow A(1,6)$ band. The $(2,5)$ and $(2,6)$ bands are contaminated by several N_2 bands, and the $(2,7)$ band is contaminated by the $E \rightarrow A(0,5)$ band. The $(0, v'')$ bands with $v''=0, 2, 3, 5-9$, the $(1, v'')$ bands with $v''=2, 9, 10$, and the $(2,4)$ band were all masked by other N_2 bands, therefore we do not report the cross sections for these bands.

The variation of the $x \rightarrow a'(2,0)$ emission cross section with respect to the incident electron energy is shown in Fig. 3. The excitation function exhibits a peak at about 32 eV. The $x \rightarrow a'(2,0)$ data has been corrected for overlap by the $a \rightarrow X(4,12)$ band. The estimated uncertainty in the values of the $(2,0)$ emission cross sections relative to the peak value is about 10% in the energy range 20–100 eV and about 15% at higher and lower energies. The $(2,0)$ band signal at 500 eV was indistinguishable from the background. Also included in Fig. 3 is our measured excitation function of the $x \rightarrow a'(1,7)$ emission band for energies up to 150 eV. The shape of this excitation function agrees very well with that of the $x \rightarrow a'(2,0)$ band. The $x \rightarrow a'(1,7)$ band is contaminated by the $c'_4 \rightarrow a(4,4)$ band which contributes appreciably to the observed emission signal at energies above 150 eV. Because of the uncertainty associated with correcting for the band overlap using method B, the $x \rightarrow a'(1,7)$ emission cross sections above 150 eV are subject to a higher percentage error and are not shown in Fig. 3.

The dependence of the $x \rightarrow a'(1,7)$ signal on N_2 pressure and electron beam current has been investigated, and the polarization of the $(1,7)$ signal has been measured. The pressure dependence of the $(1,7)$ signal has been measured at 32 eV with a beam current of 300 μA

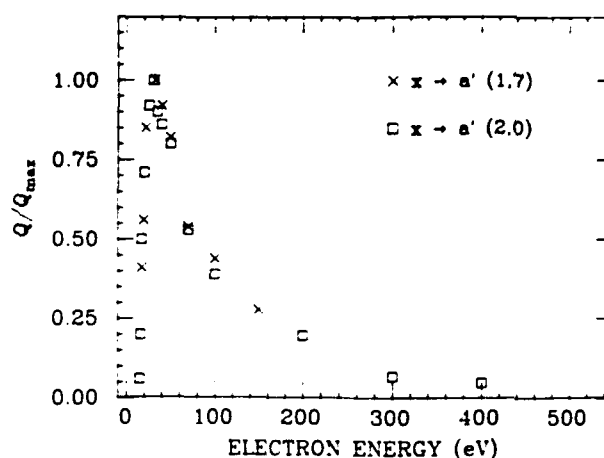


FIG. 3. Ratio of the optical-emission cross section Q to its peak value Q_{max} as a function of the incident electron energy (excitation function) for the $x \rightarrow a'(2,0)$ band (\square) and the $x \rightarrow a'(1,7)$ band (\times).

over the pressure range 1–10 mTorr. We find that the observed signal exhibits a slightly supralinear dependence on N_2 pressure in this range. The nonlinear dependence of the signal on pressure may be due to the contribution of the $c'_4 \rightarrow a(4,4)$ band to the observed signal. We have previously observed that the $c'_4 \rightarrow a(4,1)$ emission exhibits a nonlinear dependence on N_2 pressure above 0.5 mTorr.⁸ Below a pressure of 2 mTorr the $(1,7)$ signal deviates from a linear dependence on pressure by less than 5%. The maximum emission cross section of the $x \rightarrow a'(1,7)$ band has been measured at pressures of less than 2 mTorr to minimize the effect of the nonlinearity of the signal dependence on pressure. We have also checked the pressure dependence of the $x \rightarrow a'(1,8)$, $(2,0)$, and $(2,8)$ emission signals. The emission signals of all of these bands depend linearly on pressure up to 11 mTorr. The dependence of the $(1,7)$ signal on electron beam current at 32 eV has been measured over the current range 50–400 μA , and we find that the signal depends linearly on beam current in this range. The $x \rightarrow a'$ emission cross sections reported in this paper were measured with electron beam currents of less than 350 μA . We have checked the polarization of the $(1,7)$ emission at an energy of 32 eV, and we find no detectable polarization.

C. $o_3^1\Pi_u$ state

In Fig. 4 we show our measured excitation function of the $o_3 \rightarrow a(0,0)$ band. The curve has a broad peak at about 75 eV and decreases slowly at higher energies. This band is contaminated by the $A \rightarrow X(5,9)$ band; however, the emission from the $A \rightarrow X(5,9)$ band is probably not observable in our experiment due to the long lifetime of the A state. We have looked for emission signals from the $A \rightarrow X(5,5)$ and $(5,6)$ bands, but the emission signals of these two bands are not distinguishable from the background signal. The value of the $o_3 \rightarrow a(0,0)$ emission cross section at 75 eV is $(0.40 \pm 0.15) \times 10^{-21}$ cm². The estimated uncertainty in the values, plotted in Fig. 4, of the $(0,0)$ emission cross section relative to the value of the

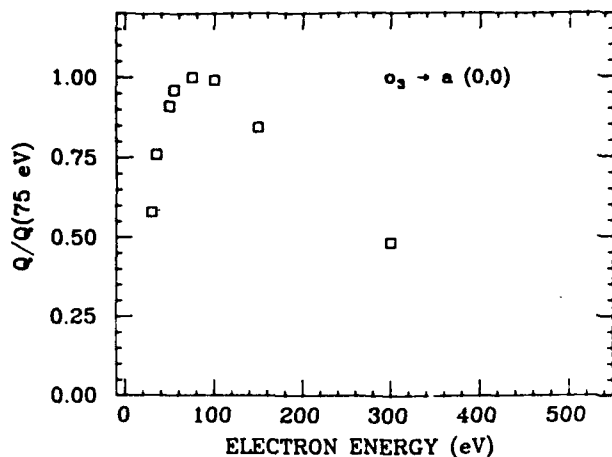


FIG. 4. Ratio of the optical-emission cross section Q to its value at 75 eV, $Q(75 \text{ eV})$, as a function of the incident electron energy (excitation function) for the $o_3 \rightarrow a(0,0)$ band.

emission cross section at 75 eV is about 25% between 35 and 150 eV and about 40% at higher and lower energies. The high uncertainty in the $o_3 \rightarrow a(0,0)$ emission cross sections is due to the very weak signal and the uncertainty in the corrections for overlap (method *A*) by adjacent N_2 bands.

We have also attempted to measure the cross section of the $o_3 \rightarrow a(0,1)$ band; however, this band is contaminated by the $y \rightarrow w(0,5)$ band. The $o_3 \rightarrow a(0,1)$ band is a red-degraded band and the $y \rightarrow w(0,5)$ band is a violet-degraded band, according to Ref. 1. The combined $o_3 \rightarrow a(0,1)$ and $y \rightarrow w(0,5)$ emission peak appears violet-degraded in our spectral scans, therefore we believe that a large part of the observed emission signal is due to the $y \rightarrow w(0,5)$ band. To estimate the $o_3 \rightarrow a(0,1)$ cross section we have calculated the Franck-Condon factors for the $o_3 \rightarrow a$ band system based on the RKR potential for the $a \ ^1\Pi_g$ state given in Ref. 1 and the RKR potential for the o_3 state given in Ref. 13. The Franck-Condon factors for the $o_3 \rightarrow a$ band system and Eq. (1) predict that the ratio of the $o_3 \rightarrow a(0,1)$ and $(0,0)$ emission cross sections is 0.24. This ratio and the value of the $(0,0)$ emission cross section at 75 eV, determined in this work, give an estimated value for the $(0,1)$ emission cross section at 75 eV of about $0.1 \times 10^{-21} \text{ cm}^2$. The relative values of the $o_3 \rightarrow a(0,1)$ and $(0,0)$ bands, however, may differ significantly from the ratio predicted by Eq. (1) due to the interaction between the $o_3 \ ^1\Pi_u$, $b \ ^1\Pi_u$, and $c \ ^1\Pi_u$ states.¹³

IV. DISCUSSION

The $x \ ^1\Sigma_g^-$, $y \ ^1\Pi_g$, and $o_3 \ ^1\Pi_u$ states of N_2 are Rydberg states with an $N_2^+(A \ ^2\Pi_u)$ ion core. Their electron MO configurations are

$$(1\sigma_g)^2(1\sigma_u)^2(2\sigma_g)^2(2\sigma_u)^2(1\pi_u)^3(3\sigma_g)^2(R)$$

where $R = 3p\pi_u$, $4p\sigma_u$, and $3s\sigma_g$ for the x , y , and o_3 states, respectively. Excitation from the ground electron-

ic state $X \ ^1\Sigma_g^-$ to the three Rydberg states corresponds to the one-electron transitions $1\pi_u \rightarrow 3p\pi_u$, $1\pi_u \rightarrow 4p\sigma_u$, and $1\pi_u \rightarrow 3s\sigma_g$. The dipole-allowed character of the $X \ ^1\Sigma_g^- \rightarrow o_3 \ ^1\Pi_u$ transition is reflected in the shape of the excitation function of the $o_3 \rightarrow a$ emission band in Fig. 4, i.e., the broad peak and the slow decline at high energy. The $X \ ^1\Sigma_g^- \rightarrow y \ ^1\Pi_g$ transition is an electric quadrupole transition. Thus the excitation function of the $y \rightarrow a'$ emission (Fig. 2) shows a narrower peak (compared to the $o_3 \rightarrow a$ excitation function) and a characteristic $1/E$ dependence at high energies. The $x \ ^1\Sigma_g^-$ state differs from $y \ ^1\Pi_g$ in that under the Born approximation, excitation from the ground state ($X \ ^1\Sigma_g^-$) to $x \ ^1\Sigma_g^-$ has zero cross section because of symmetry ($+ \rightarrow -$) even though the one-electron transition $1\pi_u \rightarrow 3p\pi_u$ associated with this excitation is of electric quadrupole type. Electron-impact excitation of the $x \ ^1\Sigma_g^-$ state can be pictured as the result of indirect coupling (by the incident electron) of the $X \ ^1\Sigma_g^-$ state with the $x \ ^1\Sigma_g^-$ state via intermediate states since direct coupling is symmetry-forbidden. (A similar situation exists in the cases of the $a' \ ^1\Sigma_u^-$ state of N_2 and numerous states of the Ne atom.^{14,15}) The excitation function of the $x \rightarrow a'$ emission in Fig. 3 has a peak similar to that found in the $y \rightarrow a'$ data in Fig. 2, but the $x \rightarrow a'$ curve appears to have a steeper descent at energies above 50 eV.

With the emission cross sections compiled in Table I, it is possible to test whether they conform closely to Eq. (1). To this end we calculate Franck-Condon factors for the $y \rightarrow w$, $y \rightarrow a'$, and $x \rightarrow a'$ transitions. In Ref. 1 a vibrational potential (RKR type) is given for the a' state. We have calculated an RKR potential for the $v' = 0-11$ vibrational levels of the w state. These RKR potentials are extended by joining them to the Morse potential functions with the correct dissociation energy for large values of internuclear distance, R , and to a function $b + a/R$ for small R values. The y state undergoes a homogeneous interaction with the $k \ ^1\Pi_g$ state. We have calculated an RKR potential for the $v' = 0,1,2$ levels of the y state based on the deperturbed molecular constants r_e , ω_e , $\omega_e x_e$, B_e , α_e , and T_e of the y state and the term values of the $v' = 0,1,2$ levels given in Ref. 16. Equations (1), (4), and (5) of Ref. 17 were employed to calculate the turning points of the vibrational levels. The RKR potential was extended to larger and smaller values of R by joining a Morse function with a dissociation energy given by $D_e = \omega_e^2 / 4\omega_e x_e$ to each side of the RKR potential. A similar procedure is used to determine the vibrational potential function for the x state. The vibrational wave functions for the a' , w , x , and y electronic states are calculated by a numerical solution of Schrödinger's equation based on Numerov's method, and the Franck-Condon factors are obtained by numerical integration. For comparison, we have also constructed an alternative set of vibrational potential functions for the x and y electronic states based entirely on the Morse function and the molecular constants r_e , ω_e , and $\omega_e x_e$ rather than using the RKR approach. The Franck-Condon factors derived from these new potentials for the x and y states (along with the RKR potentials for the a' and w states) will be

TABLE II. Franck-Condon factors of the RKR type and Morse (M) type for the $y^1\Pi_g \rightarrow w^1\Delta_u$, $y^1\Pi_g \rightarrow a'^1\Sigma_u^+$, and $x^1\Sigma_u^- \rightarrow a'^1\Sigma_u^-$ band systems. The RKR-type Franck-Condon factors were calculated using RKR potentials for the x , y , w , and a' states. The Morse-type Franck-Condon factors were calculated using Morse potentials for the x and y states and RKR potentials for the w and a' states. A blank in the entries means that the Franck-Condon factor is less than 0.001.

v'	Type	0	1	2	3	4	5	6	7	8	9
$y^1\Pi_g \rightarrow w^1\Delta_u$											
0	RKR	0.226	0.291	0.227	0.135	0.068	0.031	0.013	0.005	0.002	0.001
	M	0.254	0.298	0.220	0.126	0.060	0.026	0.010	0.004	0.001	
1	RKR	0.386	0.049	0.021	0.115	0.147	0.118	0.076	0.043	0.022	0.011
	M	0.433	0.025	0.044	0.137	0.146	0.104	0.060	0.030	0.013	0.006
2	RKR	0.274	0.090	0.155	0.025	0.010	0.068	0.102	0.095	0.070	0.045
	M	0.254	0.186	0.129	0.002	0.041	0.100	0.107	0.081	0.049	0.026
$y^1\Pi_g \rightarrow a'^1\Sigma_u^+$											
0	RKR	0.177	0.265	0.231	0.155	0.088	0.045	0.021	0.010	0.004	0.002
	M	0.202	0.276	0.228	0.146	0.080	0.039	0.017	0.007	0.003	0.001
1	RKR	0.355	0.089	0.002	0.074	0.129	0.127	0.094	0.059	0.034	0.018
	M	0.407	0.061	0.013	0.098	0.138	0.118	0.079	0.045	0.023	0.010
2	RKR	0.301	0.036	0.154	0.059		0.035	0.082	0.096	0.083	0.060
	M	0.295	0.106	0.156	0.023	0.011	0.069	0.101	0.093	0.066	0.040
$x^1\Sigma_u^- \rightarrow a'^1\Sigma_u^-$											
0	RKR	0.159	0.252	0.232	0.163	0.097	0.052	0.025	0.012	0.005	0.002
	M	0.160	0.253	0.232	0.162	0.096	0.051	0.025	0.012	0.005	0.002
1	RKR	0.343	0.108		0.060	0.121	0.127	0.099	0.065	0.038	0.020
	M	0.346	0.107		0.062	0.122	0.127	0.098	0.064	0.037	0.020
2	RKR	0.307	0.021	0.155	0.073	0.001	0.027	0.076	0.096	0.086	0.064
	M	0.307	0.023	0.157	0.071	0.001	0.029	0.078	0.097	0.086	0.062

referred to as Morse type and the set of Franck-Condon factors mentioned earlier will be referred to as RKR type. These two sets of Franck-Condon factors are given in Table II. The Morse and RKR potentials for the x state are virtually identical; therefore the two sets of $x \rightarrow a'$ Franck-Condon factors are nearly the same. The Morse and RKR potentials for the y state are slightly different, and the two sets of $y \rightarrow w$ and $y \rightarrow a'$ Franck-Condon factors, where they are greater than 0.01, generally differ by less than 20%, as shown in Table II.

Combining Eq. (1) with the appropriate Franck-Condon factors yields approximate relative values of the emission cross sections for the series of (v', v'') bands of a given v' . We normalize the cross section(s) of one (or more) member(s) of the series to the best available experimental values to obtain "Franck-Condon cross sections." Two sets of such cross sections corresponding to the RKR-type and Morse-type Franck-Condon factors are presented in Table I. The experimental cross sections that are used for normalization are marked by an asterisk in Table I. The agreement between the Franck-Condon cross sections and the experimental cross sections is, in most cases, within the experimental uncertainty and the variance between the two sets of Franck-Condon factors.

Since the $y \rightarrow w$ and $y \rightarrow a'$ Franck-Condon cross sections are based on a deperturbed vibrational potential for the y state, one must examine whether the relative intensities

of the $y \rightarrow w$ and $y \rightarrow a'(v', v'')$ bands are significantly affected by the interaction of the $y^1\Pi_g$ and $k^1\Pi_g$ states. Let us think of the perturbed $y(v')$ state as the unperturbed $y(v')$ state plus an admixture of the $k(v')$ state. The perturbed $y \rightarrow w(v', v'')$ transition moment is likewise partitioned into an unperturbed $y \rightarrow w$ term and a $k \rightarrow w$ admixture term. Because the $y \rightarrow w$ transition involves only one active electron, whereas the $k \rightarrow w$ transition involves two active electrons, the transition moment of the $k \rightarrow w$ transition should be much smaller than that of the unperturbed $y \rightarrow w$ transition. For the purpose of calculating relative intensities of the $y \rightarrow w(v', v'')$ bands for a given v' , one can therefore neglect the admixture of the $k^1\Pi_g$ state and simply use the $y(v')$ vibrational wave functions associated with the deperturbed potential. The same holds true also for the $y \rightarrow a'(v', v'')$ bands. This conclusion is indeed borne out by the reasonable agreement between the experimental cross sections and the Franck-Condon cross sections.

The $y^1\Pi_g$ state is capable of downward one-electron electric-dipole transitions to the $o_3^1\Pi_u$, $c_4^1\Sigma_u^+$, $w^1\Delta_u$, and $a'^1\Sigma_u^-$ states. The $y \rightarrow o_3$ and $y \rightarrow c_4$ transitions are in the infrared ($\lambda \sim 1.1 \mu\text{m}$) and are therefore very likely to have much smaller transition probabilities than the $y \rightarrow w$ and $y \rightarrow a'$ transitions ($\lambda \sim 0.22 \mu\text{m}$). An optical transition from $y^1\Pi_g$ to $c_3^1\Pi_u$ is also possible, but since

it involves two active electrons, it should be much weaker. Thus we expect $y \rightarrow w$ and $y \rightarrow a'$ to be the major radiative channels of the y state. An estimate of the apparent excitation cross sections of the $y(v')$ state can be obtained by summing the $y \rightarrow w(v', v'')$ and $y \rightarrow a'(v', v'')$ emission cross sections over v'' . This yields 3.8×10^{-20} , 8.2×10^{-20} , and 1.4×10^{-20} cm² for $v'=0, 1, 2$, respectively, at 32 eV. Similarly, we argue that radiative decay of the x state proceeds mainly through the $x \rightarrow a'$ transition. Our estimate for the apparent excitation cross section of the $x(v'=2)$ level is 5.7×10^{-20} cm² at 32 eV. The apparent excitation cross section is the sum of the direct excitation cross section and cascade from the higher levels. Our experiment does not provide information about the relative magnitudes of the two contributions. The o_3 state is optically connected to the ground state $X^1\Sigma_g^+$; thus the $o_3 \rightarrow X$ transition ($\lambda \sim 760$ Å) is expected to be the major radiative decay mechanism. We are unable to estimate the apparent excitation cross section of the o_3 state from our $o_3 \rightarrow a$ optical data because of the very small branching ratio of the $o_3 \rightarrow a$ emission as compared to that of the $o_3 \rightarrow X$ emission which is not measured in our experiment. The very small peak emission cross section of the $o_3 \rightarrow a(0,0)$ band determined in this work (0.4×10^{-21} cm²) as compared with the much larger $o_3 \rightarrow X(0,0)$ and $(0,2)$ emission cross sections (2.4×10^{-19} and 1.8×10^{-19} cm², respectively at 200 eV) reported in Ref. 6 confirms that the branching ratio of the $o_3 \rightarrow a$ emission is very small.

ACKNOWLEDGMENTS

The authors wish to thank R. Laher for calling our attention to the importance of the emission from the x and y states in atmospheric studies and for valuable comments and suggestions. This work was supported by the U.S. Air Force Office of Scientific Research.

APPENDIX

The $y \rightarrow w(0,2)$ band is contaminated at low energies by an unidentified molecular band. The combined excitation function of these two bands peaks near 16 eV and decreases rapidly between 16 and 32 eV. Between 32 and 100 eV the combined excitation function has the same energy dependence as the excitation functions of the $y \rightarrow w(1,3)$ and $y \rightarrow a'(1,3)$ bands. Above 100 eV, the $y \rightarrow w(0,2)$ emission signal appears to be influenced by the $N_2^+ D \rightarrow A(5,4)$ band; the combined excitation function exhibits a small, broad, secondary peak at around 200 eV, in contrast to the excitation function of the $y \rightarrow a'(1,3)$ band shown in Fig. 2. The appearance of the $y \rightarrow w(0,2)$ band shape in our spectral scans of this band also differs in the three energy ranges indicated above. Below 32 eV, the $y \rightarrow w(0,2)$ band appears to have a stronger emission band with a narrower bandwidth superimposed on it. Between 32 and 100 eV, the $y \rightarrow w(0,2)$ band shape is very similar to the band shape of the nearby $y \rightarrow w(1,3)$ band. Above 100 eV, the $y \rightarrow w(0,2)$ band again appears to have another emission band of similar intensity superimposed on it. The value of the $y \rightarrow w(0,2)$ cross section listed in Table I was measured at 32 eV. Based on the similarity of the band shapes of the $y \rightarrow w(0,2)$ and $y \rightarrow w(1,3)$ bands at 32 eV observed in our spectral scans and the similarity of the $y \rightarrow w(0,2)$ and $y \rightarrow w(1,3)$ excitation functions between 32 and 100 eV, we believe that less than 10% of the observed emission signal, at 32 eV, of the combined $y \rightarrow w(0,2)$ band and unidentified emission band is due to the unidentified band. Based on the difference, at high energies, between the excitation function of the combined $y \rightarrow w(0,2)$ and $N_2^+ D \rightarrow A(5,4)$ bands and the excitation function of the $y \rightarrow a'(1,3)$ band and on our data for the $N_2^+ D \rightarrow A(7,8)$ excitation function, we estimate that the contribution of the $D \rightarrow A(5,4)$ band to the observed $y \rightarrow w(0,2)$ emission signal at 32 eV is negligible.

¹A. Lofthus and P. H. Krupenie, *J. Phys. Chem. Ref. Data* **6**, 113 (1977).

²C. R. Hummer and D. J. Burns, *J. Chem. Phys.* **67**, 4062 (1977).

³A. Chutjian, D. C. Cartwright, and S. Trajmar, *Phys. Rev. A* **16**, 1052 (1977).

⁴S. Trajmar, D. F. Register, and A. Chutjian, *Phys. Rep.* **97**, 219 (1983).

⁵E. C. Zipf and R. W. McLaughlin, *Planet. Space Sci.* **26**, 449 (1978).

⁶H. D. Morgan and J. E. Mentall, *J. Chem. Phys.* **78**, 1747 (1983).

⁷A. R. Filipelli, S. Chung, and C. C. Lin, *Phys. Rev. A* **29**, 1709 (1984).

⁸J. S. Allen and C. C. Lin, *Phys. Rev. A* **39**, 383 (1989).

⁹K. P. Huber and G. Herzberg, *Molecular Spectra and Molecu-*

lar Structure IV. Constants of Diatomic Molecules (Van Nostrand Reinhold, New York, 1979).

¹⁰R. F. Holland, *J. Chem. Phys.* **51**, 3940 (1969).

¹¹W. Benesch, J. T. Vanderslice, S. G. Tilford, and P. G. Wilkinson, *Astrophys. J.* **143**, 236 (1966).

¹²J. M. Ajello and D. E. Shemansky, *J. Geophys. Res.* **90**, 9845 (1985).

¹³D. Stahel, M. Leoni, and K. Dressler, *J. Chem. Phys.* **79**, 2541 (1983).

¹⁴S. Chung and C. C. Lin, *Phys. Rev. A* **6**, 988 (1972).

¹⁵F. A. Sharpton, R. M. St. John, C. C. Lin, and F. E. Fajen, *Phys. Rev. A* **2**, 1305 (1970).

¹⁶P. K. Carroll and K. V. Subbaram, *Can. J. Phys.* **53**, 2198 (1975).

¹⁷A. L. G. Rees, *Proc. Phys. Soc.* **59**, 998 (1947).